Hearing Research 442 (2024) 108947

Contents lists available at ScienceDirect

Hearing Research

journal homepage: www.elsevier.com/locate/heares

Research Paper

Rational design of a genomically humanized mouse model for dominantly inherited hearing loss, DFNA9

Dorien Verdoodt [a,b,1], Erwin van Wijk [c,1], Sanne Broekman [c], Hanka Venselaar [d], Fien Aben [a,c], Lize Sels [a], Evi De Backer [a,e], Hanne Gommeren [a], Krystyna Szewczyk [a], Guy Van Camp [f], Peter Ponsaerts [b], Vincent Van Rompaey [a,e,1], Erik de Vrieze [c,1,*]

[a] Department of Translational Neurosciences, Faculty of Medicine and Health Sciences, University of Antwerp, Antwerp, Belgium
[b] Laboratory of Experimental Hematology, Vaccine and Infectious Disease Institute (Vaxinfectio), University of Antwerp, Antwerp, Belgium
[c] Department of Otorhinolaryngology, Hearing and Genes, Radboud University Medical Center, Nijmegen, GA 6525, the Netherlands
[d] Department of Medical BioSciences, Radboud University Medical Center, Nijmegen, GA 6525, the Netherlands
[e] Department of Otorhinolaryngology and Head & Neck Surgery, Antwerp University Hospital, Antwerp, Belgium
[f] Center for Medical Genetics, University of Antwerp, Antwerp 2000, Belgium

ARTICLE INFO

Keywords:
DFNA9
Genetic modification
Pre-mRNA splicing
Humanized mouse model
Hearing loss

ABSTRACT

DFNA9 is a dominantly inherited form of adult-onset progressive hearing impairment caused by mutations in the *COCH* gene. *COCH* encodes cochlin, a crucial extracellular matrix protein. We established a genomically humanized mouse model for the Dutch/Belgian c.151C>T founder mutation in *COCH*. Considering upcoming sequence-specific genetic therapies, we exchanged the genomic murine *Coch* exons 3–6 for the corresponding human sequence. Introducing human-specific genetic information into mouse exons can be risky. To mitigate unforeseen consequences on cochlin function resulting from the introduction of the human *COCH* protein-coding sequence, we converted all human-specific amino acids to mouse equivalents. We furthermore optimized the recognition of the human *COCH* exons by the murine splicing machinery during pre-mRNA splicing. Subsequent observations in mouse embryonic stem cells revealed correct splicing of the hybrid *Coch* transcript. The inner ear of the established humanized *Coch* mice displays correctly-spliced wild-type and mutant humanized *Coch* alleles. For a comprehensive study of auditory function, mice were crossbred with C57BL/6 $Cdh23^{753A>G}$ mice to remove the $Cdh23^{ahl}$ allele from the genetic background of the mice. At 9 months, all humanized *Coch* genotypes showed hearing thresholds comparable to wild-type C57BL/6 $Cdh23^{753A>G}$ mice. This indicates that both the introduction of human wildtype *COCH*, and correction of $Cdh23^{ahl}$ in the humanized *Coch* lines was successful. Overall, our approach proved beneficial in eliminating potential adverse events of genomic humanization of mouse genes, and provides us with a model in which sequence-specific therapies directed against the human mutant *COCH* alle can be investigated. With the hearing and balance defects anticipated to occur late in the second year of life, a long-term follow-up study is ongoing to fully characterize the humanized *Coch* mouse model.

1. Introduction

Affecting about 20 % of the global population, hearing loss represents the most frequent sensory deficit in humans (WHO, 2023). Regardless of the cause, hearing loss significantly impacts communication, education and employment, and it is the primary modifiable risk factor for developing dementia (Jiang et al., 2023; Shan et al., 2020). No disease-modifying therapies are available to slow down or prevent progressive sensorineural hearing loss from happening. Current management of hearing loss is therefore focused on hearing rehabilitation, primarily addressing symptoms. Patients experience the burden of progressive hearing loss before hearing aids or cochlear implants are fitted. Although these devices have a significant effect on speech understanding, they do not always lead to normal speech understanding, especially in noisy environments (Van Rompaey, 2020).

Many cases of hearing loss are caused by a genetic defect. A genetic

* Corresponding author.
E-mail address: erik.devrieze@radboudumc.nl (E. de Vrieze).
[1] These authors contributed equally to this work.

https://doi.org/10.1016/j.heares.2023.108947
Received 9 October 2023; Received in revised form 4 December 2023; Accepted 30 December 2023
Available online 31 December 2023

etiology has been reported for over 50 % of cases in children. The genetics of adult-onset hearing loss are much more complicated due to the influence of environmental factors that can damage auditory function. Nevertheless, heritability has been suggested for 31−47 % of age-related hearing loss cases (Christensen et al., 2001; DeStefano et al., 2003; Karlsson et al., 1997; Tu and Friedman, 2018). Although the minority of hearing loss cases display an autosomal dominant inheritance pattern, these usually present with a post-lingual to adult onset of progressive hearing loss. Not only can these disorders provide unique insights into the molecular mechanisms that may also underly age-related hearing loss (or presbycusis), the onset of progression of hearing loss provides a window of opportunity to deliver (genetic) treatments that aim to slow or halt disease progression in an early state.

To this day, animal models are essential to understand the pathophysiology of hearing loss, as well as to develop novel treatments. Despite the fact that several other animal species display a higher level of anatomic similarity to the human cochlea (e.g. guinea pigs, sheep and primates), mice models have become indispensable in unraveling the molecular mechanism underlying auditory function, and in the investigation of novel methods to treat hearing loss (Ohlemiller, 2019; Reiss et al., 2022). Using a combination of reverse genetics and targeted genetic manipulation, this field has established a collection of hundreds of mice strains suffering from a wide array of hearing loss disorders (Bowl et al., 2017; Ohlemiller et al., 2016). However, the large majority of these models carry either loss-of-function alleles, or mouse-specific missense variants. Very few of these models are specifically developed for the assessment of human mutation-specific genetic treatments.

Humanized mice, originally defined as mice engrafted with functional human cells or tissues, have become instrumental to investigate the function of human cells or tissues in the context of a live organism (Fujiwara, 2018). More recently, the term humanized mouse is also used to describe mouse models in which human genes, or orthologous variants associated with inherited disorders, have been introduced. In the current era of (sequence-specific) genetic therapies, these genetically humanized mouse models provide a valuable tool to investigate the molecular and therapeutic efficacy of genetic therapies targeting the human genome or transcriptome, in an animal model. The most simplified humanized mouse models carry only the (orthologous) human pathogenic variant, in an otherwise murine gene. For example, the orthologue of c.1325G>*A* (p.C442Y) has been introduced in the murine *Myo6* gene as a means to investigate the semi-dominant inheritance pattern of hearing loss in humans carrying this variant (Wang et al., 2019). And although the term humanized was not used in the paper, the knock-in mouse model for the DNFA9-associated c.263G>*A* (p.G88E) mutation in *COCH* used the same principle (Robertson et al., 2008). With this approach, the ability to investigate sequence-specific therapeutics critically depends on the similarity of the sequences flanking the variant of interest. A more elegant approach is the introduction of larger fragments the human gene of interest, as was done to establish the mouse model for a cryptic splice site mutation associated with Usher Syndrome type 1c (Lentz et al., 2007). In theory, one could replace the entire murine gene by the human ortholog with a hearing loss mutation. We have no knowledge of mouse models for hearing loss that have been established using this approach. For other disorders, such as Huntington's Disease (HD) and Duchenne Muscular Dystrophy (DMD), mouse models have been established by the transgenic delivery of the complete human genomic sequence of the disease-associated gene (Gray et al., 2008; Hoen et al., 2008). Advantage of these models is the presence of the complete human genomic sequence, allowing for the preclinical investigations of RNA- and DNA-targeting therapeutic strategies. For HD in particular, breeding of mice transgenic for human wild-type and mutant *HTT* gene with mice carrying loss of function alleles, resulted in a highly elegant model in which the targeting of mutant *HTT* through *in cis* SNPs can be studied (Southwell et al., 2013). The approach taken to develop these models also has its limitations. The human transgenes are not introduced at the endogenous locus, and the complete regulatory landscape of these genes is therefore not recapitulated. Secondly, pre-mRNA splicing of human transcripts does not necessarily have the same outcome in murine cells as in human cells, which potentially limits the feasibility of this strategy for many target sequences (Garanto et al., 2013). Note that the aforementioned HD and DMD mouse models do not appear to be affected by any of the above limitations, and both have earned their stripes in translational research, as have many other mouse models in which point mutations orthologous to human disease-associated variants have been successfully introduced. The different strategies used to develop these models highlight the increasingly important considerations in the development of humanized mouse models. Especially for animal models in which researchers aim to simultaneously address pathophysiological research questions, and replicate the human genetic situation for preclinical research on sequence-specific genetic therapies.

DFNA9 is a form of dominantly inherited hearing loss and vestibular dysfunction caused by pathogenic missense variants in the *COCH* gene. In Belgium and the Netherlands, we estimate that over 1500 people carry the c.151C>T founder mutation in *COCH*, making this mutation one of the most frequent causes of autosomal dominant hearing loss in our region. Lacking curative treatments for DFNA9, we aim to develop a genetic therapy that can prevent the formation of the mutant cochlin protein, which is assumed to cause DFNA9 through a non-haploinsufficiency disease mechanism (de Vrieze et al., 2021; JanssensdeVarebeke et al., 2018). In view of the dominant inheritance pattern, and efforts to develop a therapeutic strategy that specifically targets mutant (and not wild-type) *COCH*, it is of the utmost importance to develop a mouse model that carries both the humanized mutant, and humanized wild-type *Coch* alleles. In addition, we previously identified that c.151C>T in *COCH* is part of a shared haplotype with a low population frequency, which contains several other variants that can serve as therapeutic targets (de Vrieze et al., 2021). Lastly, DFNA9 is caused by amino acid changes in the cochlin protein. Although highly conserved between human and mouse, there are amino acids that differ between both species. The introduction of human amino acids into murine cochlin can potentially affect protein function. Considering the aforementioned successes and limitations of introducing human sequence in the genome of an animal model, there is a fine line between success and failure.

Here, we present our rational design and risk reduction strategy used to develop a genomically humanized DFNA9 mouse model for the *COCH* the c.151C>T allele. In line with previous references to Beethoven for the *Tmc1* mouse model of hearing loss, we named our humanized mutant mouse strain "*elise*" (after one of Ludwig von Beethoven's most popular compositions. To establish this mouse model, we exchanged the genomic murine *Coch* exons 3–6 for the corresponding human wild-type and mutant sequence. This allows us to evaluate sequence-specific genetic treatments directed against the mutant, human *COCH* sequence. We converted all human-specific amino acids to mouse equivalents and further refined the recognition of human *COCH* exons in mouse cochlear cells. Subsequent observations in mouse embryonic stem cells revealed correct splicing of the hybrid *Coch* transcript, which was found to be recapitulated in the inner ears of the eventual mouse models. For a comprehensive study of auditory function in this model, mice were crossbred with C57BL/6 *Cdh23*$^{753A>G}$ mice to remove the *ahl* allele which is associated with progressive age-related hearing loss. Preliminary data on auditory function indicates that *Cdh23*^{ahl}-associated hearing loss precedes the (anticipated) hearing loss caused by the c.151C>T mutation. Furthermore, the *Cdh23*^{ahl} does not appear to alter auditory function in the genomically humanized mutant *Coch* mice. The presented approach can be broadly applied to the development of humanized animal models for any disorder.

2. Material and methods

2.1. Sequences and sequence alignments

Genomic sequences are annotated on reference genomes GRCh38/hg38 (human) and GRCm39/mm39 (mouse). Human *COCH* transcript and cochlin protein sequences used in this work are NM_001135058.2 and NP_001128530.1. Mouse *Coch* transcript and cochlin protein sequence used are NM_007728 and NP_031754.1. T-Coffee web server was used to generate multiple sequence alignments (https://www.ebi.ac.uk/Tools/msa/tcoffee/) (Tommaso et al., 2011).

2.2. In silico 3D modeling of human and mouse cochlin

3D-models for both human and mouse cochlin were obtained from the AlphaFold Protein Structure Database (Jumper et al., 2021; Varadi et al., 2021). Subsequent analysis and comparison was performed using the YASARA & WHAT IF twinset (Krieger et al., 2002).

2.3. Cloning of constructs

The *COCH* minigene construct was cloned using Gateway cloning technology (Invitrogen, Carlsbad, USA). The genomic region (including *in cis* SNPs, see de Vrieze et al., 2021) of wild-type and c.151C>T mutant human *COCH* exons 3 to 7 (transcript variant 1; NM_001135058.2) were amplified using Gateway-adapted primers 5′-CCACGGCTTTAATT TTCTCATC-3′ and 5′-CACCAACCAAGAGAATATGG-3′ and cloned in a pDONR201 vector. After sequence validation, the insert was cloned into the previously published Gateway-adapted pCI-NEO splice vector (Yariz et al., 2012). Site-directed mutagenesis PCRs were performed to produce the vectors with the variants in the splice-acceptor and splice donor sites, and subsequently to recode the protein-coding sequence of human *COCH* towards murine cochlin. In brief, primers were designed to have the variant of interest flanked up- and downstream by 12–15 nt of sequence complementary to the original vector. Primers were used to amplify the original vector for 12–15 cycles using Phusion high fidelity polymerase (#M0530L, New England Biolabs, Ipswich, MA, USA). Amplified vectors were transformed in DH5α cells (#18263012, Invitrogen, Waltham, MA, USA) after DpnI (#R0176L, New England Biolabs) digestion to eliminate template vectors. After extraction and sequence verification of the resulting plasmid, subsequent mutagenesis reactions were performed until all changes were introduced. The resulting hybrid wild-type and mutant *COCH* sequences are provided in supplementary file S1. To clone the hybrid sequence between the flanking murine *Coch* sequence in expression vector pcDNA3, GeneArt seamless cloning (#A14606, Invitrogen) was used. All fragments (backbone, upstream murine *Coch*, hybrid *COCH* and downstream murine *Coch*) were amplified using primers 5′-TCCCAGTCCCTC GACTGTGCCTT-3′ and 5′-GAGGGCATCCCTATAGTGAGTCGTATT-3′ (pcDNA3), 5′-CTATAGGGATGCCCTCGTCCAGG-3′ and 5′-TCACTGCAG TCTCTCCCACGAGG-3′ (murine *Coch*), 5′-GGAGAGACTGCAGTGATG CAATCATAGCTCAT-3′ and 5′-TAGCTTACCTTTATTGCCAGTTTTCT TC-3′ (hybrid *COCH*), 5′-CAATAAAGGTAAGCTAATTGCTCGG-3′ and 5′-AGTCGAGGGACTGGGACTCACTATG-3′ (murine *Coch*). The final vector is shown in Fig. S2.

2.4. In-vitro splice assays

Murine cochlea precursor cell line UB-OC1, kindly donated by Matthew Holley, was cultured at 33 °C in high-glucose DMEM supplemented with 10 % fetal calf serum, 1 % penicillin/streptomycin, 1 mM sodium pyruvate and 50 U/mL of γ-Interferon (Rivolta et al., 1998). Transfections were performed in 6-well plates. At 60–70 % confluency, cells were transfected with 1 μg of pcNEO splice vector or pcDNA3 hybrid *COCH* vector using polyethylenimine as previously described for HEK293T cells (Roosing et al., 2014). After 24 h, cells were harvested for transcript analysis.

2.5. Transcript analysis

Total RNA from UB-OC1 cells and murine embryonic stem cells was extracted with the Nucleospin RNA kit (#740955, Machery-Nagel, Düren, Germany) according to the manufacturer's instructions. To extract RNA from mouse temporal bones, samples were homogenized in Trizol™ (#15596026, Invitrogen) using a Bio-Gen PRO200 Homogenizer (#01–01200, PRO scientific, Oxford, CT, USA) Next, RNA Trizol extraction was performed according to the manufacturer's instructions, followed by a second clean-up of the RNA sample using the Nucleospin RNA kit. The obtained RNA was reverse transcribed using the iScript cDNA synthesis kit (#1708891, Bio-Rad, Hercules, CA, USA). To investigate pre-mRNA splicing, part of the cDNA was amplified under standard PCR conditions using Q5 polymerase (New England Biolabs, #M0491L, Ipswich, MA) and primers 5′-CGGAGGTCAACAACGAGTCT-3′ and 5′-AGGTGTAGGGGATGGGAGAC-3′ (recognizing exons 3 and 5 of the human *RHO* gene) or primers 5′-ACGTGTGGTCCTTCTGTTCC-3′ and 5′-CAGGATCCCTGCTCTCTGC-3′ (recognizing murine exons 1 and 7). Primers 5′-ACTGGGACGACATGGAGAAG-3′ and 5′- TCTCAGCTGTG GTGGTGAAG-3′, recognizing mouse *Actb*, were used for amplification controls. Quantitative PCR of all *Coch* transcripts, regardless of humanization, was done using GoTaq qPCR mix (#A6002, Promega, Madison, WI, USA) and primers 5′-TTGCATTTGTTGACAAGGCTGT-3′ and 5′-CCAAACCAGTTGGGCATGTG-3′. These primers recognize exon 9 and 10 which are identical between all mouse strains. Expression is normalized to an index of three housekeeping genes calculated by Bestkeeper (Pfaffl et al., 2004). Primers to amplify the housekeeping genes are *Eef2* (5-'TGTCAGTCATCGCCCATGTG-3′ and 5′-CATCCTTG CGAGTGTCAGTGA-3′), *Rpl37* (5′- CCAAGCGCAAGAGGAAGTATAA-3′ and 5′- CATGTCTGAATCTGCGGTAGAC-3′) and *Gapdh* (5′-CTCCCA CTCTTCCACCTTCG-3′ and 5′-GCCTCTCTTGCTCAGTGTCC-3′). The humanized mutant and wild-type alleles are amplified using an allele-specific Taqman™ assay as previously published (de Vrieze et al., 2021). G-blocks with wild-type and mutant PCR targets were used to calculate transcript levels per μg RNA as previously described (Dulla et al., 2021).

2.6. Generation of the mouse lines

The humanized wild type, floxed *Coch* and humanized mutant, floxed *Coch* mouse models were developed by genOway (Lyon, France) by replacing mouse *Coch* genomic sequence from intron 2 to the exon 6 by its human counterpart, either wild type or harboring the c.151C>T (p.P51S) point mutation in human exon 3 (mouse counterpart of human p.P51 is p.P53). Single nucleotide polymorphisms (SNP) rs12432528:T, rs1124181:C, rs143609554:T, rs7140538:T, rs7140258:A, rs10701465: dupAG were included to the mutant sequence. In addition, the rs1124181:C SNP was included to both the wild-type and mutant models. The presence of loxP sites flanking the humanized region provides the opportunity to generate a knock-out allele. The *Coch* gene targeting vectors were constructed from genomic C57BL/6 N mouse strain DNA and fully sequenced to confirm vector integrity. Linearized targeting vector was transfected into C57BL/6 ES cells according to GenOway's electroporation procedures. G-418 resistant ES cell clones were subsequently validated by PCR, using primers hybridizing within and outside the targeted locus, and whole locus sequencing to confirm the absence of any genetic alteration. Recombined ES cell clones were microinjected into C57BL/6 blastocysts, and gave rise to male chimeras with a significant ES cell contribution. Breedings were established to remove the Neomycin cassette and produce the humanized wild type, floxed and humanized mutant, floxed *Coch* mouse lines. These heterozygous animals were genotyped by PCR, and further validated by full sequencing of the Coch locus, including the homology arms. The resulting humanized wild-type allele has been deposited at the mouse

genome informatics database (MGI) as *Coch<tm1(COCH)Geno>* (MGI reference: 7441,935). The humanized c.151C>T mutant allele has been deposited as *Coch<tm2(COCH*P51S)Geno>* (MGI reference: 7441,936). For the mutant line, the synonym *Elise* was deposited after the popular name for Beethoven's Bagatelle No. 25 in A minor (*Für Elise*).

2.7. Elimination of the $cdh23^{ahl}$ locus

C57BL/6 mice are known to suffer from age-related hearing loss (ahl) resulting from the c.753G>*A* mutation in the *Cdh23* gene. As the overall goal is to develop a long-term model, we backcrossed the generated humanized *COCH* mice to the C57BL/6 ($Cdh23^{753A>G}$) background, in which the mutation that leads to ahl has been successfully corrected (Mianné et al., 2016). This backcrossing resulted in 6 different strains that are subject of further investigation in current and future work (Table 1).

2.8. Visualization of cochlin in the spiral ligament

Mice were euthanized with an overdose of pentobarbital (200 mg/ml). The skull of the mouse was cut open with scissors and brain tissue was removed to expose the temporal bones bilaterally. The otic capsule and surrounding tissue was removed so a small incision could be made in the apex. The cochleae were fixated in 4 % paraformaldehyde (PFA) for 1 h. Afterwards, they were washed 3 × 5 min with PBS and incubated in 0.5 M EDTA overnight. The cochleae were washed with PBS and incubated in increasing sucrose concentrations (2 h in sucrose 5 %, 2 h in sucrose 10 % and overnight in sucrose 20 %). Next, cryosectioning was performed in the desired orientation and the sections were washed with PBS for 3 × 5 min and placed in 0.1 % Triton X-100 for 30 min, followed by an incubation in blocking solution (20 % goat serum and 20 % donkey serum in PBS) for 1 h. The slices were incubated overnight with a rat monoclonal anti-Cochlin primary antibody at 4 °C (1:200; #MABF267, clone 9A10D2, Merck Millipore, Burlington, MA, USA). Next sections were washed 4 × 3 min with PBS after which they were incubated for 1 h at room temperature with a goat anti-rat Alexa Fluor 488 secondary antibody (1:1000; #A11006, Invitrogen) in blocking solution. Then the sections were washed again with PBS, and incubated with DAPI (1 μg/ml, Sigma) in PBS for 10 min. Afterwards, the samples were washed 2 × 2 min with demineralized water and mounted in ProLong™ Gold Antifade (#P10144, Invitrogen). Sections were visualized using Olympus BX51 fluorescence microscope equipped with an Olympus DP71 digital camera. Olympus CellSens software was used for image acquisition and processing.

2.9. Hearing assessments

Long-term follow-up of auditory function in all seven strains is currently ongoing (starting with $n = 40$ per group). Subsets of animals are sacrificed at selected timepoints throughout the long-term phenotypic follow-up that will be part of subsequent publication. Here, we present the result of the hearing assessment obtained in adult mice at 9 months of age in equal numbers of males and females. Since DFNA9 and *Cdh23*-related hearing loss are late-onset disorders, conducting hearing assessments at earlier stages lacks meaningful significance.

2.9.1. Anesthesia

Mice were anesthetized with an intraperitoneal (i.p.) injection with a ketamine (100 mg/kg body weight) and xylazine (20 mg/kg body weight) mixture. Reflexes were assessed by a hind limb withdrawal reflex. In case mice did not reach an areflexive state, boosters of ketamine/xylazine one-fifth of the original dose were administered fifteen minutes after anesthesia induction. Hearing assessment was started five minutes after ketamine/xylazine injection. After anesthesia induction, mice were individually placed in a sound-attenuating chamber (Industrial Acoustic Company, North Aurora, IL, USA) on a homeothermic heating pad system (Harvard Apparatus, Holliston, MA, USA) to maintain constant body temperature (37 ± 0.5 °C). Prior to each recording session, ophthalmic ointment (Duratears, Alcon, Geneva, Switzerland) was applied to the eyes to prevent corneal drying.

2.9.2. Distortion Product Otoacoustic Emissions (DPOAE)

Anesthetized mice were placed on their left flank under a device securely holding an acoustic probe tightly fitted into the right external auditory canal. Two tones (f1 and f2) were administered simultaneously in the right ear only via a close-field method. DPOAE responses (2f1−f2) were measured over a frequency range from 5 to 32 kHz, more specifically at 4, 4.5, 5.2, 6, 6.9, 8.0, 9.2, 10.6, 12.1, 13.9, 16.0, 18.4, 21.1, 24.3, 27.9, and 32.0 kHz. The primary tone ratio f2/f1 was set to 1.22. DPOAE responses were evoked by a non-symmetric DPOAE protocol, using unequal primary tone stimulus intensities (i.e., L1 > L2). Five intensity levels were presented with L1 going from 70 to 30 dB SPL and L2 = L1 − 10 dB SPL. Duration of testing was approximately 10 min per animal. To enable statistical analysis and calculations of the mean, unobtainable DPOAE thresholds at our equipment's limits of 70 dB SPL were defined as 80 dB SPL.

2.9.3. Auditory Brainstem Responses (ABR)

Evoked responses were recorded using disposable subcutaneous needle electrodes (28 G) positioned over the vertex of the skull (active electrode), the left mastoid (reference electrode) and the right hindlimb (ground electrode). Evoked potentials were measured after administration of frequency-specific sound stimuli through a free-field electrostatic speaker placed 10 cm in front of the animal's head. BioSig32 software (Tucker-Davis Technologies, Alachua, FL, USA) was used to generate tone burst stimuli of 2 msec in length with a gate of 1 msec at frequencies 4, 8, 16, 32 and 41 kHz in 5 dB steps starting at 90 dB SPL down to a minimum SPL of 10 dB. A stimulus repetition rate of 32 per second was used and 800 trials were recorded for each frequency to obtain a good averaged response. ABR thresholds were defined as the lowest stimulus level at which any reproducible ABR waveform could be reliably

Table 1
humanized wild-type and c.151C>T mutant Coch mouse strains.

Strain name	*full name*	*description*
$Coch^{hWT/hWT}Cdh23^{cor}$	B6N(Cg)-*Cdh23*<ahl+em3H> *Coch*<tm1.1(*COCH*)Geno>/Ant	Mice homozygous for the wild-type humanized *Coch* allele and the $Cdh23^{753A>G}$ correction
$Coch^{hP51S/hP51S}Cdh23^{cor}$	B6N(Cg)-*Cdh23*<ahl+em3H> *Coch*<tm2.1(*COCH*P51S)Geno>/Ant	Mice homozygous for the c.151C>T (p.P51S) mutant humanized *Coch* allele and the $Cdh23^{753A>G}$ correction
$Coch^{hWT/hP51S}Cdh23^{cor}$		Biallelic humanized mouse with the wild-type and mutant *Coch* allele in compound heterozygosity, and homozygous for the $Cdh23^{753A>G}$ correction
$Coch^{hWT/hWT}Cdh23^{ahl}$		Mice homozygous for the wild-type humanized *Coch* allele and the $Cdh23^{ahl}$ allele
$Coch^{hP51S/hP51S}Cdh23^{ahl}$		Mice homozygous for the c.151C>T (p.P51S) mutant humanized *Coch* allele and the $Cdh23^{ahl}$ allele
$Coch^{hWT/hP51S}Cdh23^{ahl}$		Biallelic humanized mouse with the wild-type and mutant *Coch* allele in compound heterozygosity, and homozygous for the $Cdh23^{ahl}$ allele

observed in the evoked response at appropriate latencies upon visual inspection and was determined by comparing the ABR waveforms with several suprathreshold ABRs. In addition, amplitudes of wave I were assessed at all frequencies. Upon completion of testing, needle electrodes were removed, and animals were moved individually to heated cages and monitored until complete recovery. Duration of testing was approximately 30 min per animal. To enable statistical analysis and calculations of the mean, unobtainable ABR thresholds at our equipment's limits of 90 dB SPL were defined as 95 dB SPL.

2.10. Statistics

Statistical analyses were done in Graphpad Prism (Graphpad Software, Boston, MA, USA). One-way ANOVA with Tukey's posttest was performed on gene expression data. Since audiometry data was not normally distributed, Kruskal Wallis tests were performed to analyze hearing thresholds between the different mouse strains at 9 months of age.

3. Results and discussion

3.1. COCH gene and cochlin protein are highly conserved between human and mouse

In order to design the humanized *COCH* mouse model, we first compared the *COCH* gene and cochlin protein between human and mouse. The human *COCH* gene is located on chromosome 14, and contains 11 protein-coding exons. Besides the reference transcript (transcript variant 1, NM_001135058.2; Fig. 1A), several alternative transcripts have been described within the GENCODE project (Frankish et al., 2018), of which the biological relevance remains unclear. Most noteworthy is transcript variant 3 (NM_001347720) containing a 195 bp extension of exon 2, which has been found in human cochlear and vestibular cells at comparable levels to transcript variant 1 (Schrauwen et al., 2016). The murine *Coch* gene is found on chromosome 12, and has only two annotated transcripts within GENCODE, both of which translate into the same cochlin amino acid sequence. Transcript variant 1 (NM_007728) has the same intron-exon structure as shown in Fig. 1A, whereas transcript variant 2 (NM_001198835) has an alternatively spliced 5′UTR.

The encoded cochlin protein is composed of multiple protein domains (Fig. 1B). The signal peptide, shown green, is encoded by exon 1. The LCCL (Limulus factor C, Coch-5b2 and Lgl1) domain is encoded by exons 2–5 and contains several DFNA9-associated missense variants, including the founder mutation c.151C>T. Cochlin furthermore contains two vWFA (von Willebrand factor type A) domains, which are encoded by exons 6 to 10 (vWFA1) and exons 10 and 11 (vWFA2), as shown in red in Fig. 1B. The amino acid sequence of human and mouse cochlin is highly similar (94 % sequence identity). Comparison of the 3D protein models of human and mouse cochlin also reveals a very high degree of structural similarity (Fig. 1C), both in the overall folding of the protein, and in the region of the proline residue at position 51 (position 53 in mice). Replacing the proline with a serine, as results from the c.151C>T (p.P51S) mutation in *COCH*, is predicted to affect both the human and mouse cochlin protein in the same manner. Interestingly, the 3D models suggest that the P51S mutation does not induce a

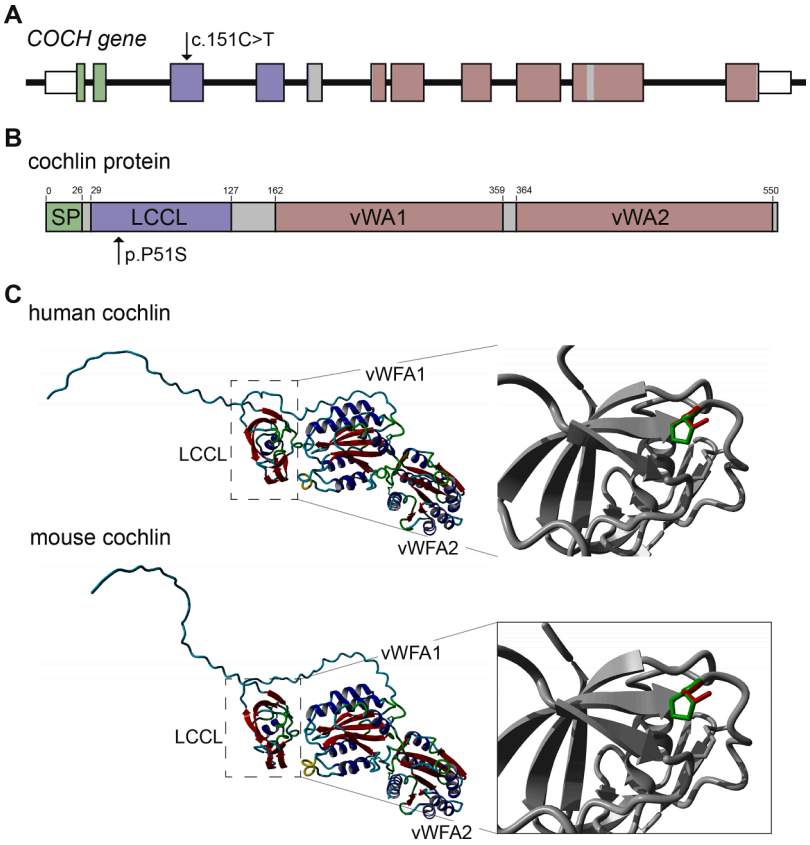

Fig. 1. Composition of the *COCH* gene and cochlin protein. (**A**) Graphical representation of the human *COCH* intron-exon structure. The colors correspond to the protein domains encoded by the different exons, as shown in (B). (**B**) Protein domain architecture of human cochlin, showing the signal peptide (SP) in green, the Limulus factor C, Coch-5b2 and Lgl1 (LCCL) domain in blue, and the two von Willebrand Factor A domains (vWFA) in red. The numbers indicate the amino acids boundaries based on the Alphafold 2 models. (**C**) 3D models of human and mouse cochlin proteins. Both proteins fold in a highly similar and typical manner in which the LCCL and vWFA domains can be clearly distinguished. Details of the LCCL domains of human and mouse cochlin show proline 51 (proline 53 in mouse) in green, and the DFNA9-associated serine in red, and underline the high degree of similarity of both mutant and wild-type cochlin between both species.

conformational change to the LCCL domain in either species. The two cysteines flanking P51 are likely to form a disulphide bond that anchors the structure of the domain, on which the P51S change is predicted to have little effect. This contradicts previous literature suggesting that the P51S amino acid substitution causes misfolding of the protein (Bae et al., 2014; Liepinsh et al., 2001; Yao et al., 2010). The work of Robertson and co-workers, investigating the intracellular localization and secretion of mutant cochlin in mammalian cells, is more in line with our conclusions from the 3D protein models as they suggest that the deleterious effects of several DFNA9 mutations (including P51S, V66G and G88E) primarily

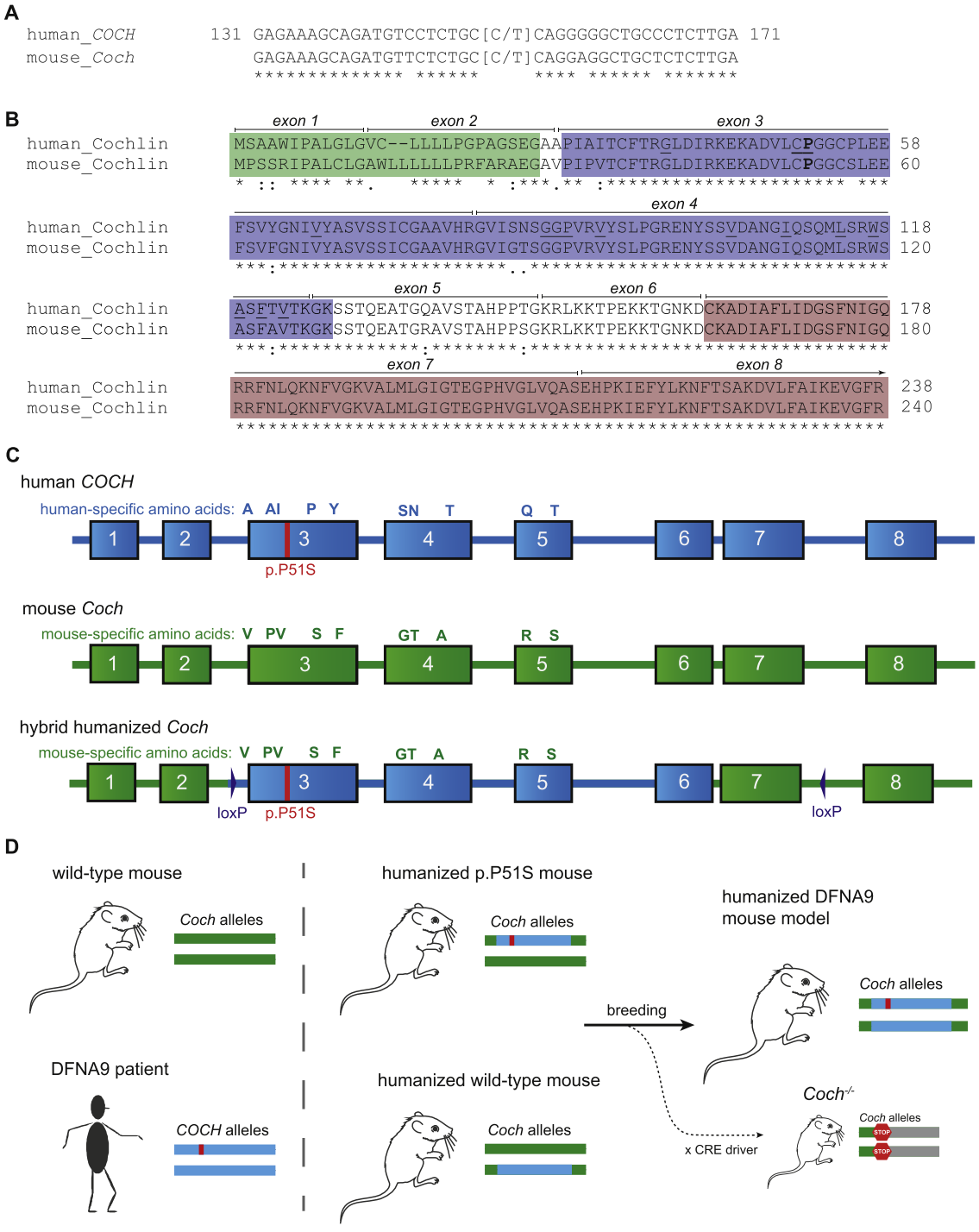

Fig. 2. Rational design of the humanized P51S cochlin mouse model. (**A**) Sequence alignment of human *COCH* and murine *Coch* sequences flanking human cytosine 151 (shown in bold). Three nucleotide differences can be observed in the 20 nucleotides upstream and downstream of cytosine 151, revealing the limitation of testing sequences specific therapeutics. (**B**) Alignment of human and mouse cochlin amino acid sequence encoded by exons 1 to 8. The proline at position 51 is highlighted in bold. Amino acid residues that, when mutated, lead to DFNA9 are underlined. The background colors are in line with the cochlin protein domains as visualized in Fig. 1B. (**C**) Graphic representation of the human and mouse *COCH* allele, and of the amino acids that different between species. Human sequence is indicated in blue, mouse in green. The hybrid humanized *Coch* fragment depicts the humanization of exons 3–6, with retention of mouse-specific amino acid sequence. LoxP sites are introduced in intron 2 and intron 6. (**D**). Representation of the different alleles and breeding strategy towards the final humanized DNFA9 mouse model carrying both alleles in heterozygosity. Breeding of these mice with a CRE driver line leads to a mouse strain carrying premature stop codons in *Coch*.

occur beyond the point of secretion, in the unique environment of the extracellular matrix of the inner ear (Robertson et al., 2003). Regardless of the consequences of the P51S substitution on cochlin function, the observed similarity in 3D protein models between human and mouse suggests that we can indeed investigate the molecular consequences of P51S when introducing the orthologous amino acid substitution in mouse.

3.2. Design of hybrid humanized Coch alleles with recoded amino acids to avoid potential changes to cochlin function in the humanized mouse

First and foremost, our humanized *Coch* mouse model should allow for the investigation of human-specific therapies that aim to block the production of P51S cochlin in a sequence-specific manner. This means that (1) the sequence flanking the human c.151C>T variant should be introduced in the mouse, and (2) a second strain is required carrying corresponding human wild-type allele to assess allele-specificity of such therapeutics. The nucleotides immediately up- and downstream of position 151 in human *COCH* are largely identical to the murine counterparts (Fig. 2A). There are however 3 nucleotides that differ between human and mouse, which are likely to be part of the targeting sequence of genome-editing and antisense oligonucleotides therapeutics. In addition, we previously identified several genetic variants with a low population frequency that are *in cis* with the c.151C>T mutation, which could therefore serve as alternative therapeutic targets (de Vrieze et al., 2021). To investigate therapeutics directed against SNPs on the mutant allele, it is important to also introduce (some of) these variants into the mouse model. The variant in intron 5 (c.436+368_436+369dupAG, rs10701465), is particularly interesting to include in the mouse model as it creates a larger difference between both alleles than a single nucleotide change.

Although we would ideally replace the complete mouse *Coch* gene with the human orthologue, this would also alter the cochlin amino acid sequence. More than 20 amino acid substitutions have been described to result in DFNA9 (Verdoodt et al., 2020), but the molecular mechanism underlying these mutations remains uncertain. As such, it is virtually impossible to predict if we can replace mouse-specific amino acids of cochlin for the human counterparts without altering protein function. For this reason, we also quickly rejected transgenic introduction of the complete human *COCH* gene using a similar approach as previously used to establish humanized mouse models for e.g. Duchenne Muscular Dystrophy (DMD) and Huntington's Disease (HD) (Gray et al., 2008; Hoen et al., 2008).

Alternatively, we investigated the option to generate hybrid humanized *Coch* alleles (coined $Coch^{hWT}$ and $Coch^{hP51S}$), a strategy that has been very successful in the past, for example in the development of both a murine and porcine model for Usher syndrome type 1c (Grotz et al., 2022; Lentz et al., 2007). We defined the target fragment of the wild-type and mutant human *COCH* gene to span from exon 3 (containing c.151C) to exon 6 (in order to include the SNP in intron 5). This will result in the humanization of the complete LCCL domain of cochlin and, if unaddressed, the introduction of 10 human-specific amino acids in the mouse cochlin protein (Fig. 2B). To eliminate even the slightest chance that the introduction of the human-specific amino acids interferes with normal cochlin function, we decided to recode the 10 human-specific amino acids back to the murine triplets. As a result, the final hybrid humanized *hCoch* alleles will encode the complete mouse cochlin amino acid sequence (wild-type or P51S) (Fig. 2C). The envisioned mouse model for DFNA9 will carry one humanized mutant allele, and one humanized wild-type allele, in compound heterozygosity (Fig. 2D). Additionally, loxP sites were introduced into the recombination template to allow for the generation of loss-of-function alleles (c.89_886del p.P31Nfs*4) after breeding the humanized mice with a CRE driver line.

3.3. Strategic adjustments to the splice donor and splice acceptor sites secure normal pre-mRNA splicing of human Coch exons in mouse inner ear cells

Previous studies revealed that species-specific differences in pre-mRNA splicing can affect the functional outcome and translational value of humanized animal models (Garanto et al., 2015; Slijkerman et al., 2018). Aiming to prevent this, we investigated pre-mRNA splicing of human *COCH* exons 3–6 in mouse inner ear cells prior to the generation of the humanized mice. We cloned the genomic sequence of *COCH* exon 3 to exon 7, and 1 kb of flanking intronic sequence between the two *RHO* exons of the midigene splice vector (Fig. 3A). Next, we transfected this vector into UB-OC1 cells, which are derived from the embryonic auditory sensory epithelia of immortomouse (Rivolta et al., 1998) to investigate recognition of the human splice sites by the splicing machinery of mouse inner ear cells (Fig. 3B). Amplification of transcripts using primers complementary to the 5′ and 3′ *RHO* exons revealed that human *COCH* exons 4 and 7 are poorly recognized by the murine splicing machinery. The majority of transcripts lacked either exon 4, exon 7, or both. Splicing of exons 3, 5 and 6 occurred similar to the reference transcripts. A second PCR, using primers directed against *COCH* exons 3 and 7, confirmed the skipping of exon 4 to be a problem for the development of a humanized mouse model (Fig. 3C). It furthermore showed that correct pre-mRNA splicing occasionally occurs in the transfected mouse cells.

Aiming to improve recognition of human *COCH* exons 4 in murine cells, we first compared the human and murine sequences of splice donor and acceptor sites, and calculated the splice-site strengths using NNSPLICE 0.9 (Reese et al., 1997). At both sites, the sequence is reasonably well conserved (Fig. 4A). At the splice acceptor site, the exon sequence is identical between human and mouse, whereas the exonic sequence of the splice donor site differs by 1 nucleotide. We previously showed that recognition of a human (cryptic) exon can be improved in zebrafish by strengthening the intronic sequence of the splice donor and splice acceptor sites (Schellens et al., 2022). In view of the predicted strengths, the human splice donor site is particularly weak (0.18, vs. 0.57 in mouse). Both the human and mouse splice acceptor site have a higher predicted strength (0.89 and 0.63, resp.). Lacking clear cut-off values for efficient splicing, we investigated options to improve the predicted splice-site strength of both sites. The previously published consensus splice acceptor and splice donor sequence of human and mouse are highly identical (Abril et al., 2005). In both human and mouse, the exonic splice acceptor sequence deviates from the canonical sequences at 2 out of 3 positions. Since changing these nucleotides would alter the encoded protein, we opted to change the intronic sequence of the acceptor site in order to better match the optimal sequence. At nearly all intronic acceptor positions, a thymine is associated with most-efficient splicing. Indeed, the introduction of 5 thymine nucleotides increased the NNSPLICE score to 0.99 (Fig. 4B). Similarly, introducing an adenine in the intronic splice donor sequences increased the NNSPLICE score to 0.97. We introduced the proposed variants into the midigene splice vector, and transfected these improved vectors in UB-OC1 cells to assess whether the inclusion of exon 4 was improved. Amplification from *RHO* exon 3 to *RHO* exon 5 revealed that introduction of the variants prevents the formation of the amplicon lacking both exon 4 and exon 7 (Fig. S3). Sequencing of the amplicons revealed that exon 4 was included in nearly all amplicons. To better visualize the improvements in pre-mRNA splicing resulting from the introduction of splice-strengthening variants in the intronic acceptor and donor sites, the *COCH* transcript was amplified from exon 3 to exon 7 (Fig. 4C). While the skipping of exon 4 was resolved by the introduced changes in the splice sites, retention of intron 6 presented as a potential problem in the generation of the humanized mouse. Additionally, a PCR from *COCH* exon 5 to *RHO* exon 5 revealed that exon 7 skipping remains a potential problem (Fig. 4D).

COCH exons 6 and 7 are separated by an intron of 90 nucleotides in

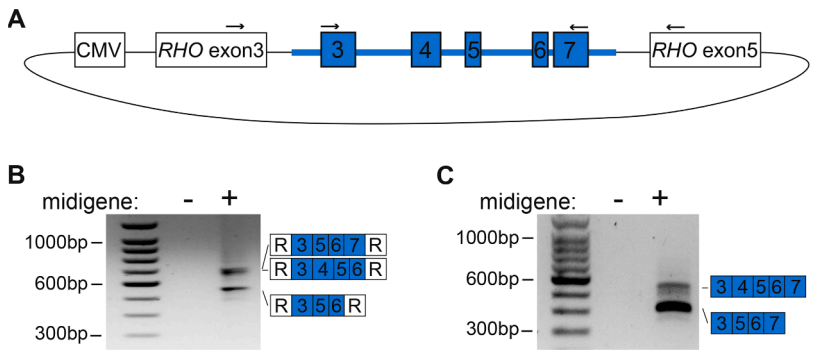

Fig. 3. Splicing of human *COCH* exons in murine inner ear cells. (**A**) Graphic representation of the midigene splice vector in which cloned the human genomic *COCH* fragment containing exons 3 to 7 between two RHO exons. Arrows indicate primer positions used to amplify midigene transcripts. (**B**) RT-PCR analysis investigating the splicing of the complete midigene reveals multiple products in which exon 4, exon 7 or both exons 4 and 7 are not included in the final transcript. (**C**) Amplification from exon 3 to exon 7 reveals that a small proportion of transcripts is correctly spliced. All amplicons were validated with Sanger sequencing.

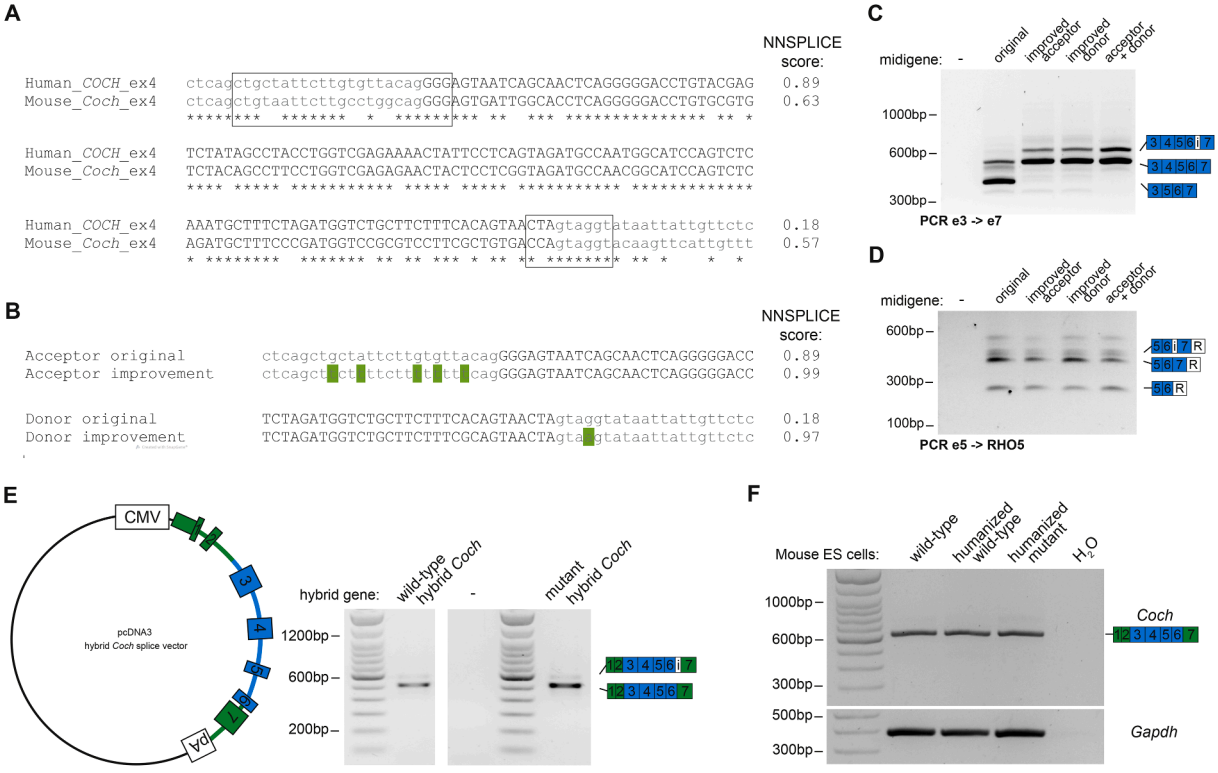

Fig. 4. Improving recognition of *COCH* exon 4 in mouse cells. (**A**) Sequence alignment of human and mouse COCH exon 4, including the splice acceptor and splice donor sites (box). NNSPLICE score is given at the end of each row with a splice site as a measure of splice site strength. (**B**) Sequence alignment of the original splice acceptor and splice donor sites, and the proposed improvements (green). (**C**) RT-PCR analysis investigating the splicing of *COCH* exons 4 to 7 shows a strong improvement in the recognition of *COCH* exon 4. Retention of intron 7 was also observed in part of the amplicons. (**D**) RT-PCR analysis using primers on *COCH* exon 5 and *RHO* exon 5 shows that skipping of exon 7 remains unaltered between the original and improved midigenes. (**E**) Plasmid map of the hybrid humanized *Coch* 5′ gene fragment used to investigate pre-mRNA splicing of human *COCH* exons within the eventual humanized transcript. RT-PCR analysis using primers on *Coch* exons 1 and 7 showed that the majority of transcripts is splice correctly, and a small proportion shows retention of intron 7. (**F**) Analysis of humanized *Coch* pre-mRNA splicing in mouse ES cell clones that were used to generate the chimeric founder mice. Wild-type ES cells were included as controls. Sanger sequencing was used to confirm the sequence of all amplicons that are schematically depicted in panels C-F.

length. Since there are no potential targets for therapy in this part of the human *COCH* gene, we hypothesized that keeping the complete mouse intron 6 and exon 7 sequence in the hybrid *Coch* allele might be the easiest solution. To investigate this, we cloned a vector encoding the final situation in the mouse genome from exon 1 to exon 7. Breakpoints between murine and human sequence were chosen in intron 2 (mouse c.89–735 -> human c.83–721) and at the first nucleotide of intron 6 (human c.481 -> mouse c.487+1). Wild-type and mutant hybrid *Coch* vectors were produced in which the human *in cis* variants of the corresponding alleles are included, and in which all human-specific amino acids were recoded to the mouse amino acids. The resulting hybrid *Coch* vectors were transfected into UB-OC1 cells to investigate splicing of the hybrid *Coch* transcript in mouse inner ear cells. Correct splicing was observed in both the wild-type and mutant hybrid transcript (Fig. 4E). This indicates that the improvement to the splice sites of exon 4 was indeed successful to secure normal splicing of the hybrid humanized

Coch transcript. A small amount of intron 6 retention also occurs in a transcript with mouse intron 6 and exon 7, while skipping of exon 7 is no longer observed. Non-sequential splicing is known to occur (Gazzoli et al., 2016), and if the removal of intron 6 occurs slightly slower and less efficient as compared to the other introns, overexpression of the hybrid *Coch* gene fragment may create a non-physiological situation in which a small amount of intron 6 retention remains visible. Regardless of the cause, we concluded that the intron 6 retention is likely a feature of the murine transcript, and therefore requires no further improvement.

Having improved the recognition of the human *COCH* exons in mouse inner ear cells as much as possible with these in-vitro assays, the template vectors containing the final sequences to be introduced into the mouse genome were shipped to GenOway, where the mice with humanized alleles were produced. The generation of a transgenic or humanized mouse cost a significant amount of time and money. Therefore, we included a final checkpoint in the development of the humanized mice, and investigated pre-mRNA splicing of the hybrid humanized *Coch* alleles in the embryonic stem (ES) cells used to produce the chimeric founder mice. The ES cells produced by GenOway were investigated for (hybrid) *Coch* pre-mRNA splicing. Although the alleles in the humanized ES cells still contain a proprietary selection cassette for transgenesis, we observed only correctly spliced amplicons in true wild-type ES cells, and in the wild-type and mutant humanized ES cells (Fig. 4F). Note that the retention of intron 6 was not observed in these cells that endogenously express the hybrid humanized *Coch* transcript.

3.4. Normal expression of hybrid humanized Coch alleles and cochlin protein in the mouse cochlea

The hybrid humanized mouse strains were delivered as F1 generation with heterozygous humanized alleles on a C57BL/6 background with the *Cdh23*^{ahl} allele. We simultaneously set up a breeding strategy to

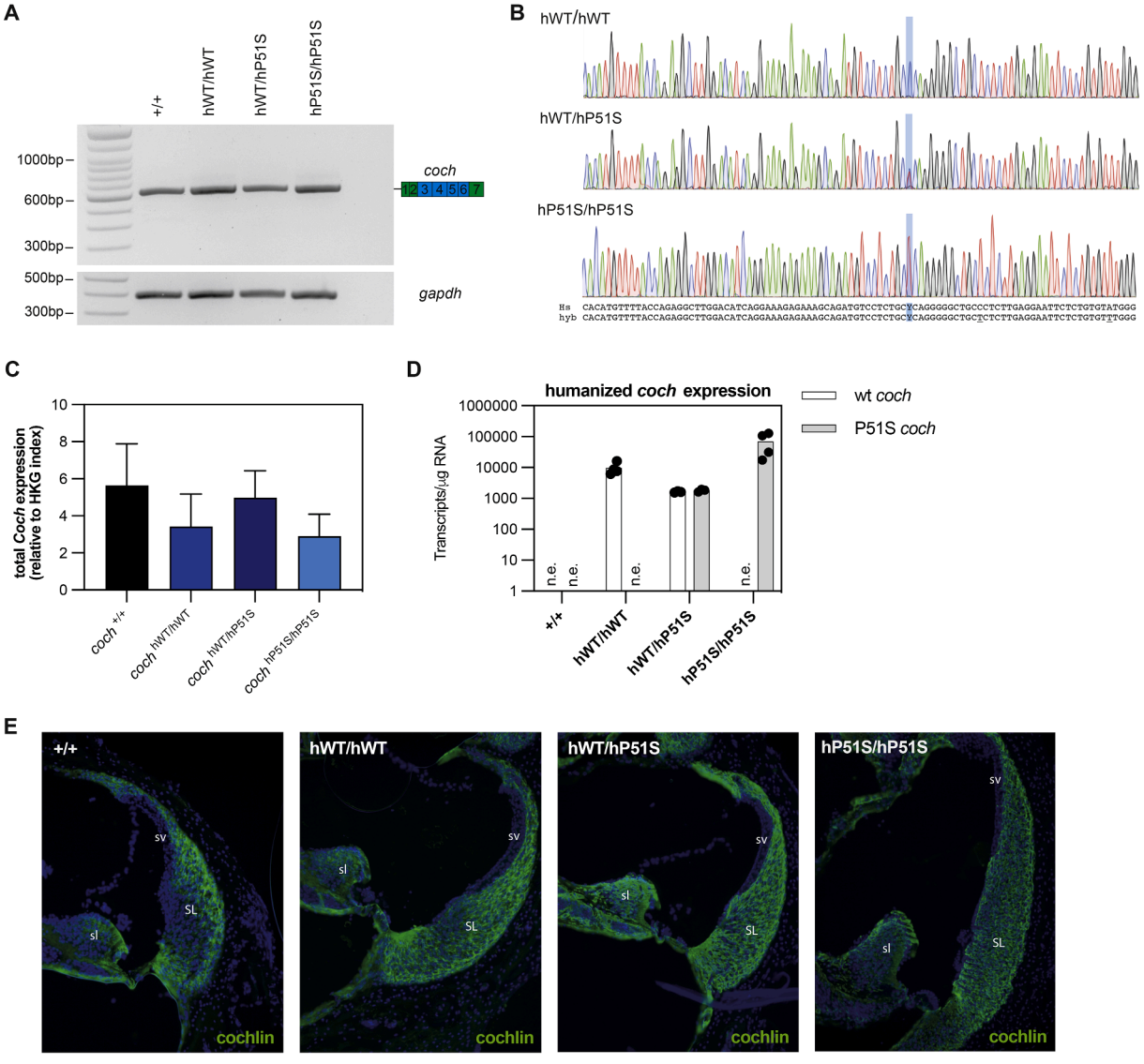

Fig. 5. Correct expression and pre-mRNA splicing of humanized *Coch* and cochlin in the mouse inner ear. (**A**) RT-PCR analysis revealing correct pre-mRNA splicing of *Coch* in all three genotypes. (**B**) Sanger sequencing traces confirming the absence or presence of the DFNA9-associated c.151C>T mutation. The original human (Hs), and hybrid (hyb) *Coch* sequence are shown below the Sanger traces. Differences between original human *COCH* and hybrid *Coch*, resulting from the recoding of human-specific amino acids, are underlined. (**C**) Quantitative analysis of total *Coch* gene expression. Normalized expression is depicted as mean ± SD. Housekeeping index contains *Eef2, Rpl37* and *Gapdh*. (**D**) Absolute qPCR of humanized wild-type and mutant *Coch* transcripts in the temporal bones of each genotype. Expression values are calculated as number of transcripts per µg RNA. Mean and individual values are displayed for those genotypes that carry the allele encoding the target transcripts. (**E**) Cochlin expression in the spiral ligament (SL) and spiral limbus (sl) of the cochlea (Cochlin antibody, green) in the different mouse strains. Stria vascularis is indicated with SV.

produce the mice as shown in Table 1, and performed a preliminary study on humanized *Coch* expression and pre-mRNA splicing. Once all genotypes had been bred, temporal bones were dissected from 5-month-old humanized mice for a thorough investigation of gene and protein expression (Fig. 5). RT-PCR analysis on mRNA isolated from temporal bones revealed a single amplicon for mouse *Coch* in complete wild-type mice. In all three genotypes of humanized mice ($Coch^{hWT/hWT}$, $Coch^{hWT/hP51S}$ and $Coch^{hP51S/hP51S}$), the same pre-mRNA splicing pattern was observed as was seen for mouse *Coch* (Fig. 5A). Note that the retention of intron 6 that was observed in the in-vitro studies was not detected in the mouse temporal bone. Sanger sequencing confirmed that the amplicons contained indeed humanized wild-type and humanized mutant *Coch* (Fig. 5B). Note that two peaks are visible at nucleotide 157 of the heterozygous humanized mice, confirming that both alleles are expressed in this strain. When comparing the Sanger traces to the human sequence, two of the nucleotide substitutions resulting from recoding the human-specific amino acids are visible downstream of the c.151C>T variant. To investigate whether humanized *Coch* and native mouse *Coch* alleles are equally expressed, a quantitative RT-PCR was conducted using primers recognizing the exons 9 and 10, which are outside the transgenic region and thus allow the amplification of *Coch* in all mouse strains. Although mild differences in total *Coch* expression can be observed between the different mouse strains, normalized transcript levels are not significantly different between strains (one-way ANOVA, Tukey's multiple comparison test) (Fig. 5C). The lowest P-value is 0.2 for the comparison between $Coch^{+/+}$ and $Coch^{hP51S/hP51S}$ samples. We furthermore observed equal expression of humanized wild-type and humanized mutant *Coch* transcripts in temporal bones of heterozygous mice (Fig. 5D). As a final confirmation that the genomic humanization was successful, cochlin protein was visualized in temporal bone slices of wild-type mice. Results showed that cochlin expression was present in the spiral ligament and spiral limbus in all the different genotypes indicating that humanization of the *Coch* gene was successful and did not have an impact on cochlin protein formation (Fig. 5E). Note that in the homozygous humanized lines, humanized wild-type and humanized mutant cochlin can be specifically visualized, whereas as mixture of both is anticipated to be visualized in the heterozygous $Coch^{hWT/hP51S}$. Specificity of the antibody is shown by the lack of anti-cochlin immunoreactivity in the cochlea of $Coch^{-/-}$ mice (Supplementary file S4). Overall, the obtained data on humanized *Coch* transcripts and cochlin protein suggest that the genomic humanization of the mouse line was successful. Although we cannot know for sure how the original human *COCH* transcript would be spliced in the murine cochlea, we conclude that the in-vitro investigation of pre-mRNA splicing, and subsequent changes to the splice donor and splice acceptor site were important to ensure normal pre-mRNA splicing of the eventual hybrid transcript. As some of the previous humanized animal models did display unforeseen problems with the recognition of human exons (Garanto et al., 2015; Slijkerman et al., 2018), our approach presents a quick and easy method to investigate splicing in a relevant cellular context, and introduce improvements if needed. The UB-OC1 cell line was selected as it is derived from the mouse cochlea, and expresses many genes related to inner ear function, including *Coch*. However, UB-OC1 cells are of an ectoderm origin, whereas *Coch*-expressing fibrocytes are derived from the mesoderm (Furness, 2019; Rivolta et al., 1998). As such, UB-OC1 cells present a valuable tool, but do not offer the exact context of the fibrocytes. It might be possible to investigate pre-mRNA splicing in fibrocytes using primary cell cultures from the cochlear lateral wall of mice, or by injectoporation of midigene construct into the mouse cochlea (Gratton et al., 1996; Xiong et al., 2014). However both options do require experimental animals, and methods for efficient delivery of midigenes into the fibrocytes have yet to be established.

3.5. Humanization of the Coch gene has no negative impact on hearing function

Based on a previous publication of a knock-in mouse model for the c.263G>*A* (p.G88E) mutation in *Coch*, onset of an auditory and vestibular phenotype is anticipated to occur between 15 and 21 months of age. Based on previously published in-vitro data on cleavage and secretion of P51S and G88E cochlin, we have no reason to assume that mice carrying the P51S mutation will develop auditory and vestibular phenotypes different from the G88E mouse. As such, the $Cdh23^{ahl}$ allele in the background of the mice in which the humanized alleles were introduced, is anticipated to result in hearing defects before the onset of a DFNA9-associated phenotype. Previous work, in which the $Cdh23^{ahl}$ allele was repaired using CRISPR-Cas9 ($Cdh23^{cor}$), revealed that 24-week-old mice carrying the *ahl* allele already display a significant increase in ABR threshold at 32 kHz as compared to mice with the corrected allele (Mianné et al., 2016). Therefore, we crossed our *hCoch* mice with $Cdh23^{cor}$ mice to remove the *ahl* allele from our mouse strains. Extensive auditory and vestibular phenotyping is ongoing. Here, we present the first results obtained in mouse of mixed sex. Outer hair cell function is assessed by performing DPOAE measurements. Our results indicate that outer hair cell function at 9 months is similar between $Cdh23^{cor}$ mice and wild-type humanized $Coch^{hWT/hWT}$ mice (Fig. 6A). Significant differences in DPOAE thresholds are observed between $Cdh23^{ahl/ahl}$ mice and the mice corrected for the *ahl* locus ($Cdh23^{cor}$) starting from 16 kHz up to 32 kHz, as expected. The exact p-values are reported in the supplementary file S5. In line with the phenotype of the G88E mice, no outer hair cell defect was observed in both heterozygous ($Coch^{hWT/hP51S}$) and homozygous ($Coch^{hP51S/hP51S}$) humanized *Coch* strains as compared to humanized wild-type controls (Fig. 6B). Since we speculated that the $Cdh23^{ahl}$ allele could accelerate the phenotype of humanized mutant *Coch* mice, we also investigated auditory function for all three humanized *Coch* genotypes in the $Cdh23^{ahl}$ background (Fig. 6C). No differences were observed between humanized wild-type and mutant strains. However, the significant differences in threshold that are observed at 16 kHz and above for all humanized *Coch* genotypes in the $Cdh23^{ahl}$ background as compared to those corrected for the *ahl* locus ($Cdh23^{cor}$), emphasize the relevance of removing the *ahl* allele. Auditory Brainstem Responses (ABRs) are an indication of auditory pathway function, from the primary auditory neurons synapsing with the sensory cells of the cochlea, the inner hair cells, to the inferior colliculus in the midbrain. ABR thresholds at 9 months of age revealed that hearing function of humanized wild-type *Coch* mice is not impaired when comparing them with $Cdh23^{cor}$ wild-types (Fig. 6D). The typical loss of high frequency hearing associated with the $Cdh23^{ahl}$ allele is visible in $Coch^{hWT/hWT}$ in which the *ahl* allele has not been repaired. Small differences can be observed between the three humanized *Coch* genotypes in $Cdh23^{cor}$ background at three out of five frequencies, but not to the extent of a hearing loss phenotype (Fig. 6E). In line with the results from the DPOAE, the ABR results also reveal significant differences between the mice corrected for the *ahl* locus on the *Cdh23* gene and mice carrying the ahl locus ($p < 0.001$, supplementary file S5) at 16 kHz, 32 kHz and 41 kHz (Fig. 6F). For clarity, DPOAE and ABR data is displayed in multiple graphs, visualizing different comparisons. Statistical analyses were performed on the entire dataset comparing all strains. Based on the Vestibular Deficit Index (VDI) which is a behavioral test battery that has been successfully used to assess the loss of vestibular function in mice (Verdoodt et al., 2021), we have no indication to suspect a vestibular defect at this age as vestibular rating scores remained within the normal control range across all groups. Nor is there any indication that the *ahl* locus on the *Cdh23* gene has an effect on vestibular functioning mice.

As hearing loss caused by the *ahl* locus starts at the highest frequencies, which is confirmed by our measurements, our results indicate that rescuing the auditory function in our corrected *hCoch* mouse model by backcrossing to the C57BL/6 ($Cdh23^{cor}$) background was successful and necessary since the onset of $Cdh23^{ahl}$-associated hearing loss

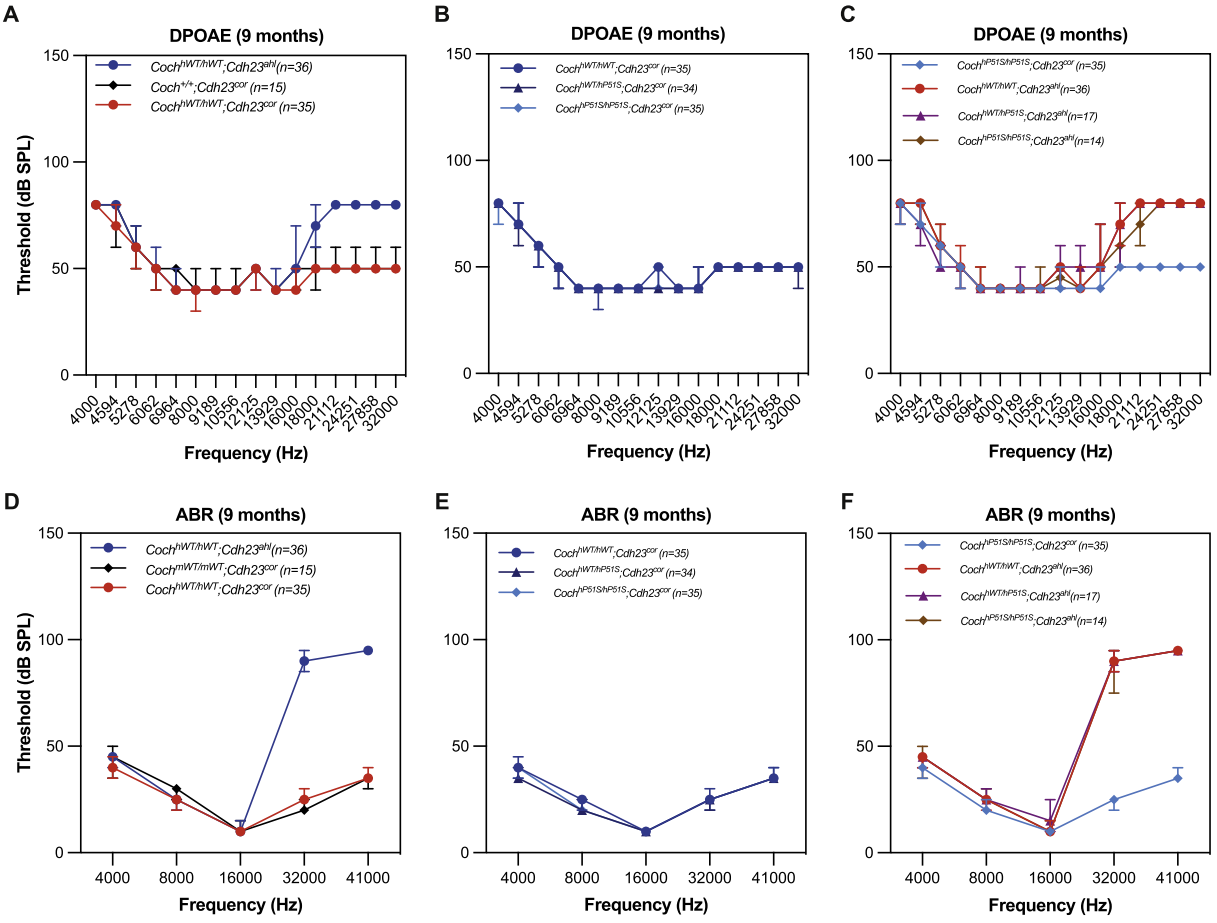

Fig. 6. Hearing assessment of our humanized mouse model. (**A**) DPOAE measurements in wild-type humanized *Coch*$^{hWT/hWT}$ mice are similar to DPOAE thresholds observed in *Cdh23*^{cor} mice but significantly different from DPOAE thresholds seen in *Cdh23*^{ahl} mice in the range of 16–32 kHz. (**B**) DPOAE measurements are similar in humanized *Coch*$^{hWT/hWT}$, *Coch*$^{hWT/hP51S}$ and *Coch*$^{hP51S/hP51S}$ mice at 9 months of age. (**C**) After 9 months, DPOAE measurements are significantly different between *Cdh23*^{cor} and *Cdh23*^{ahl} mice starting from 16 kHz to 32 kHz. (**D**) ABR measurements indicate that hearing thresholds are similar between humanized *Coch*$^{hWT/hWT}$ and *Cdh23*^{cor} mice but significantly different from hearing thresholds in *Cdh23*^{ahl} mice at 16, 32 and 41 kHz. (**E**) No significant differences are observed between humanized *Coch*$^{hWT/hWT}$, *Coch*$^{hWT/hP51S}$ and *Coch*$^{hP51S/hP51S}$ mice at 9 months of age. (**F**) ABR assessment revealed that hearing thresholds in *Cdh23*^{cor} mice significantly differ from hearing thresholds observed in *Cdh23*^{ahl} mice at 16, 32 and 41 kHz. Data are not normally distributed, and are expressed as median ± 95 % CI. Statistical analyses are provided in supplementary file S5.

precedes the (anticipated) hearing loss associated with DFNA9. C57BL/6 remains a popular laboratory strain in hearing research and beyond. The presence or absence of the *Cdh23*^{ahl} allele is assumed to have little consequences in preclinical studies using mouse models that display an early-onset or congenital hearing loss phenotype. Indeed, many successful proof-of-concept studies on novel hearing loss therapeutics have been done in C57BL/6 mice. Here, we highlight the value of removing this allele from the C57BL/6 background based on the (anticipated) age of onset of the DFNA9-associated hearing loss phenotype. Additionally, the presence of the *ahl* allele can also be problematic in long-term follow-up studies investigating novel hearing loss treatments, As the extent to which auditory defects can be rescued declines with age. Lastly, cadherin 23 (encoded by the *CDH23* gene) is a key component of the tip links of hair cell stereocilia, and as such, may influence the phenotypic outcome of hearing loss caused by other genetic variants through genetic interaction (Newton et al., 2022; Watson and Tempel, 2013). Based on the data obtained so far in our humanized *Coch* mouse model, we find no evidence of a potential genetic interaction between *Cdh23* and *Coch* variants. Ongoing phenotypic follow-up over a 2-year timeframe will reveal the extent of auditory and vestibular phenotypes, and opportunities to investigate therapeutic strategies at the level of restoring or preventing hearing loss.

4. Conclusions

To this day, animal models are crucial to understand the function of the inner ear, and to develop novel treatments for hearing loss and vestibular dysfunction. Although stem cell technology is rapidly advancing to replace animal models, even for hearing loss disorders, animal models are still superior in mimicking the complexity of the human cochlea and vestibular system. Lacking an animal model for the c.151C>T founder mutation in *COCH*, which causes DFNA9, we aimed to establish a humanized mouse model that allows for a broad spectrum of fundamental and translational pre-clinical investigations. For many mouse models for inherited diseases, only the orthologous human variant is introduced in the mouse gene. With the increasing flexibility and efficiency of genetic modification, it is now possible to introduce bigger modifications in the animal genome, allowing the development of much more sophisticated animal models that can be used to answer a wide array of fundamental and therapeutic research questions.

Following a similar as previously used murine and porcine models of inherited diseases such as Usher syndrome type 1c, we introduced the human DFNA9-associated mutation, and flanking sequence, into the mouse genome. Introducing human sequences in animal models can lead to unforeseen pre-mRNA splicing defects, this manuscript shows this can be easily identified and resolved in advance using a few simple in-vitro

assays. By introducing carefully positioned loxP sites, allowing to also generate a loss-of-function mouse model, and producing a humanized wild-type strain, we now have access to a highly elegant and versatile genomically humanized mouse model for the c.151C>T founder mutation that is causative for DFNA9. The development and breeding of mice with the ideal genotype to study DFNA9 (*Coch*$^{hWT/hP51S}$ in *Cdh23*^{cor}) took around three years. However, it now provides us with a unique model to investigate the efficiency and specificity of sequency-specific therapeutic strategies directed against the human c.151C>T allele within a fully functional, mammalian cochlea. The overall design of the mouse model, and de-risking strategy that we followed, can serve as inspiration for the development of many other animal models for human diseases.

CRediT authorship contribution statement

Dorien Verdoodt: Conceptualization, Formal analysis, Supervision, Writing – original draft, Writing – review & editing, Investigation. **Erwin van Wijk:** Conceptualization, Funding acquisition, Supervision, Writing – review & editing. **Sanne Broekman:** Investigation. **Hanka Venselaar:** Investigation, Visualization. **Fien Aben:** Investigation. **Lize Sels:** Investigation. **Evi De Backer:** Investigation. **Hanne Gommeren:** Investigation. **Krystyna Szewczyk:** Investigation. **Guy Van Camp:** Conceptualization, Funding acquisition. **Peter Ponsaerts:** Conceptualization, Funding acquisition, Supervision, Writing – review & editing. **Vincent Van Rompaey:** Conceptualization, Funding acquisition, Supervision, Writing – review & editing. **Erik de Vrieze:** Conceptualization, Funding acquisition, Investigation, Supervision, Visualization, Writing – original draft, Writing – review & editing.

Declaration of Competing Interest

The authors have no competing interests

Data availability

No data was used for the research described in the article.

Acknowledgments

We are grateful to Christel Jacobs of the Antwerp animalarium for their excellent animal husbandry, and GenOway for the pleasant collaboration during both the design and production phase of the mouse strains. This study was financially supported by “Stichting de Negende van”, “Royal National Institute for Deafness” (Flexigrant F95), and “Queen Elisabeth Medical Foundation for Neurosciences, University of Antwerp (36959, 48844), Young Universities for the Future of Europe (YUFE), Research Foundation Flanders (G034422N, 1126023N, 18E2524N).

Supplementary materials

Supplementary material associated with this article can be found, in the online version, at doi:10.1016/j.heares.2023.108947.

References

Abril, J.F., Castelo, R., Guigó, R., 2005. Comparison of splice sites in mammals and chicken. Genome Res. 15, 111–119. https://doi.org/10.1101/gr.3108805.

Bae, S.H., Robertson, N.G., Cho, H.J., Morton, C.C., Jung, D.J., Baek, J.I., Choi, S.Y., Lee, J., Lee, K.Y., Kim, U.K., 2014. Identification of pathogenic mechanisms of COCH mutations, abolished cochlin secretion, and intracellular aggregate formation: genotype-phenotype correlations in DFNA9 deafness and vestibular disorder. Hum. Mutat. 35, 1506–1513. https://doi.org/10.1002/humu.22701.

Bowl, M.R., Simon, M.M., Ingham, N.J., Greenaway, S., Santos, L., Cater, H., Taylor, S., Mason, J., Kurbatova, N., Pearson, S., Bower, L.R., Clary, D.A., Meziane, H., Reilly, P., Minowa, O., Kelsey, L., , Consortium, T.I.M.P., Allen, S., Clementson-Mobbs, S., Codner, G., Fray, M., Gardiner, W., Joynson, R., Kenyon, J., Loeffler, J., Nell, B., Parker, A., Quwailid, D., Stewart, M., Walling, A., Zaman, R., Chen, C.K., Conte, N., Matthews, P., Relac, M., Tudose, I., Warren, J., Marchand, E.L., Amri, A. E., Fertak, L.E., Ennah, H., Ali-Hadji, D., Ayadi, A., Wattenhofer-Donze, M., Moulaert, D., Jacquot, S., André, P., Birling, M.C., Pavlovic, G., Lalanne, V., Lux, A., Riet, F., Mittelhaeuser, C., Bour, R., Guimond, A., Bam'Hamed, C., Leblanc, S., Vasseur, L., Selloum, M., Sorg, T., Ayabe, S., Furuse, T., Kaneda, H., Kobayashi, K., Masuya, H., Miura, I., Obata, Y., Suzuki, T., Tamura, M., Tanaka, N., Yamada, I., Yoshiki, A., Berberovic, Z., Bubshait, M., Cabezas, J., Carroll, T., Clark, G., Clarke, S., Creighton, A., Danisment, O., Eskandarian, M., Feugas, P., Gertsenstein, M., Guo, R., Hunter, J., Jacob, E., Lan, Q., Laurin, V., Law, N., MacMaster, S., Miller, D., Morikawa, L., Newbigging, S., Owen, C., Penton, P., Pereira, M., Qu, D., Shang, X., Sleep, G., Sohel, K., Tondat, S., Wang, Y., Vukobradovic, I., Zhu, Y., Chiani, F., Pietro, C.D., Segni, G.D., Ermakova, O., Ferrara, F., Fruscoloni, P., Gambadoro, A., Gastaldi, S., Golini, E., Sala, G.L., Mandillo, S., Marazziti, D., Massimi, M., Matteoni, R., Orsini, T., Pasquini, M., Raspa, M., Rauch, A., Rossi, G., Rossi, N., Putti, S., Scavizzi, F., Tocchini-Valentini, G.D., Beig, J., Bürger, A., Giesert, F., Graw, J., Kühn, R., Oritz, O., Schick, J., Seisenberger, C., Amarie, O., Garrett, L., Hölter, S.M., Zimprich, A., Aguilar-Pimentel, A., Beckers, J., Brommage, R., Calzada-Wack, J., Fuchs, H., Gailus-Durner, V., Lengger, C., Leuchtenberger, S., Maier, H., Marschall, S., Moreth, K., Neff, F., Östereicher, M.A., Rozman, J., Steinkamp, R., Stoeger, C., Treise, I., Stoeger, T., Yildrim, A.Ö., Eickelberg, O., Becker, L., Klopstock, T., Ollert, M., Busch, D.H., Schmidt-Weber, C., Bekeredjian, R., Zimmer, A., Rathkolb, B., Wolf, E., Klingenspor, M., Tocchini-Valentini, G.P., Gao, X., Bradley, A., Skarnes, W.C., Moore, M., Beaudet, A.L., Justice, M.J., Seavitt, J., Dickinson, M.E., Wurst, W., Angelis, M.H.de, Herault, Y., Wakana, S., Nutter, L.M.J., Flenniken, A.M., McKerlie, C., Murray, S.A., Svenson, K.L., Braun, R. E., West, D.B., Lloyd, K.C.K., Adams, D.J., White, J., Karp, N., Flicek, P., Smedley, D., Meehan, T.F., Parkinson, H.E., Teboul, L.M., Wells, S., Steel, K.P., Mallon, A.M., Brown, S.D.M., 2017. A large scale hearing loss screen reveals an extensive unexplored genetic landscape for auditory dysfunction. Nat. Commun. 8, 886. https://doi.org/10.1038/s41467-017-00595-4.

Christensen, K., Frederiksen, H., Hoffman, H.J., 2001. Genetic and environmental influences on self-reported reduced hearing in the old and oldest old. J. Am. Geriatr. Soc. 49, 1512–1517. https://doi.org/10.1046/j.1532-5415.2001.4911245.x.

DeStefano, A.L., Gates, G.A., Heard-Costa, N., Myers, R.H., Baldwin, C.T., 2003. Genomewide linkage analysis to presbycusis in the framingham heart study. Arch. Otolaryngol. Head Neck Surg. 129, 285–289. https://doi.org/10.1001/archotol.129.3.285.

de Vrieze, E., Martín, J.C., Peijnenborg, J., Martens, A., Oostrik, J., Heuvel, S.van den, Neveling, K., Pennings, R., Kremer, H., Wijk, E.van, 2021. Antisense oligonucleotide-based degradation of c.151C>T mutant COCH transcripts associated with dominantly inherited hearing impairment DFNA9. Mol. Ther. Nucl. Acids 24, 274–283. https://doi.org/10.1016/j.omtn.2021.02.033. Molecular Therapy - Nucleic Acids.

Dulla, K., Slijkerman, R., Diepen, H.C.van, Albert, S., Dona, M., Beumer, W., Turunen, J. J., Chan, H.L., Schulkens, I.A., Vorthoren, L., Besten, C.den, Buil, L., Schmidt, I., Miao, J., Venselaar, H., Zang, J., Neuhauss, S.C.F., Peters, T., Broekman, S., Pennings, R., Kremer, H., Platenburg, G., Adamson, P., de Vrieze, E., Wijk, E.van, 2021. Antisense oligonucleotide-based treatment of retinitis pigmentosa caused by USH2A exon 13 mutations. Mol. Ther. 29, 2441–2455. https://doi.org/10.1016/j.ymthe.2021.04.024. Molecular Therapy.

Frankish, A., Diekhans, M., Ferreira, A.M., Johnson, R., Jungreis, I., Loveland, J., Mudge, J.M., Sisu, C., Wright, J., Armstrong, J., Barnes, I., Berry, A., Bignell, A., Carbonell Sala, S., Chrast, J., Cunningham, F., Di Domenico, T., Donaldson, S., Fiddes, I.T., García Girón, C., Gonzalez, J.M., Grego, T., Hardy, M., Hourlier, T., Hunt, T., Izuogu, O.G., Lagarde, J., Martin, F.J., Martínez, L., Mohanan, S., Muir, P., Navarro, F.C.P., Parker, A., Pei, B., Pozo, F., Ruffier, M., Schmitt, B.M., Stapleton, E., Suner, M.M., Sycheva, I., Uszczynska-Ratajczak, B., Xu, J., Yates, A., Zerbino, D., Zhang, Y., Aken, B., Choudhary, J.S., Gerstein, M., Guigó, R., Hubbard, T.J.P., Kellis, M., Paten, B., Reymond, A., Tress, M.L., Flicek, P., 2018. GENCODE reference annotation for the human and mouse genomes. Nucl. Acids Res. 47, gky955. https://doi.org/10.1093/nar/gky955.

Fujiwara, S., 2018. Humanized mice: a brief overview on their diverse applications in biomedical research. J. Cell. Physiol. 233, 2889–2901. https://doi.org/10.1002/jcp.26022.

Furness, D.N., 2019. Forgotten fibrocytes: a neglected, supporting cell type of the cochlea with the potential to be an alternative therapeutic target in hearing loss. Front. Cell Neurosci. 13, 532. https://doi.org/10.3389/fncel.2019.00532.

Garanto, A., Beersum, S.E.C.van, Peters, T.A., Roepman, R., Cremers, F.P.M., Collin, R.W. J., 2013. Unexpected CEP290 mRNA splicing in a humanized knock-in mouse model for Leber congenital amaurosis. PLoS One 8, e79369. https://doi.org/10.1371/journal.pone.0079369.

Garanto, A., Duijkers, L., Collin, R.W.J., 2015. Species-dependent splice recognition of a cryptic exon resulting from a recurrent intronic CEP290 mutation that causes congenital blindness. Int. J. Mol. Sci. 16, 5285–5298. https://doi.org/10.3390/ijms16035285.

Gazzoli, I., Pulyakhina, I., Verwey, N.E., Ariyurek, Y., Laros, J.F.J., Hoen, P.A.C.'t, Aartsma-Rus, A., 2016. Non-sequential and multi-step splicing of the dystrophin transcript. RNA Biol. 13, 290–305. https://doi.org/10.1080/15476286.2015.1125074.

Gratton, M.A., Schulte, B.A., Hazen-Martin, D.J., 1996. Characterization and development of an inner ear type I fibrocyte cell culture. Hear. Res. 99, 71–78. https://doi.org/10.1016/s0378-5955(96)00080-9.

Gray, M., Shirasaki, D.I., Cepeda, C., Andre, V.M., Wilburn, B., Lu, X.H., Tao, J., Yamazaki, I., Li, S.H., Sun, Y.E., Li, X.J., Levine, M.S., Yang, X.W., 2008. Full-length human mutant huntingtin with a stable polyglutamine repeat can elicit progressive

and selective neuropathogenesis in BACHD mice. J. Neurosci. 28, 6182–6195. https://doi.org/10.1523/jneurosci.0857-08.2008.
Grotz, S., Schäfer, J., Wunderlich, K.A., Ellederova, Z., Auch, H., Bähr, A., Runa-Vochozkova, P., Fadl, J., Arnold, V., Ardan, T., Veith, M., Santamaria, G., Dhom, G., Hitzl, W., Kessler, B., Eckardt, C., Klein, J., Brymova, A., Linnert, J., Kurome, M., Zakharchenko, V., Fischer, A., Blutke, A., Döring, A., Suchankova, S., Popelar, J., Rodríguez-Bocanegra, E., Dlugaiczyk, J., Straka, H., May-Simera, H., Wang, W., Laugwitz, K.L., Vandenberghe, L.H., Wolf, E., Nagel-Wolfrum, K., Peters, T., Motlik, J., Fischer, M.D., Wolfrum, U., Klymiuk, N., 2022. Early disruption of photoreceptor cell architecture and loss of vision in a humanized pig model of usher syndromes. Embo. Mol. Med. e14817. https://doi.org/10.15252/emmm.202114817.
Hoen, P.A.C.'t, Meijer, E.J.de, Boer, J.M., Vossen, R.H.A.M., Turk, R., Maatman, R.G.H.J., Davies, K.E., Ommen, G.J.B.van, Deutekom, J.C.T.van, Dunnen, J.T.den, 2008. Generation and characterization of transgenic mice with the full-length human DMD gene*. J. Biol. Chem. 283, 5899–5907. https://doi.org/10.1074/jbc.m709410200.
JanssensdeVarebeke, S.P.F., Camp, G.V., Peeters, N., Elinck, E., Widdershoven, J., Cox, T., Deben, K., Ketelslagers, K., Crins, T., Wuyts, W., 2018. Bi-allelic inactivating variants in the COCH gene cause autosomal recessive prelingual hearing impairment. Eur. J. Hum. Genet. EJHG 23, 42. https://doi.org/10.1038/s41431-017-0066-2.
Jiang, F., Mishra, S.R., Shrestha, N., Ozaki, A., Virani, S.S., Bright, T., Kuper, H., Zhou, C., Zhu, D., 2023. Association between hearing aid use and all-cause and cause-specific dementia: an analysis of the UK Biobank cohort. Lancet Public Heal. 8, e329–e338. https://doi.org/10.1016/s2468-2667(23)00048-8.
Jumper, J., Evans, R., Pritzel, A., Green, T., Figurnov, M., Ronneberger, O., Tunyasuvunakool, K., Bates, R., Žídek, A., Potapenko, A., Bridgland, A., Meyer, C., Kohl, S.A.A., Ballard, A.J., Cowie, A., Romera-Paredes, B., Nikolov, S., Jain, R., Adler, J., Back, T., Petersen, S., Reiman, D., Clancy, E., Zielinski, M., Steinegger, M., Pacholska, M., Berghammer, T., Bodenstein, S., Silver, D., Vinyals, O., Senior, A.W., Kavukcuoglu, K., Kohli, P., Hassabis, D., 2021. Highly accurate protein structure prediction with AlphaFold. Nature 596, 583–589. https://doi.org/10.1038/s41586-021-03819-2.
Karlsson, K.K., Harris, J.R., Svartengren, M., 1997. Description and primary results from an audiometric study of male twins. Ear Hear. 18, 114–120. https://doi.org/10.1097/00003446-199704000-00003.
Krieger, E., Koraimann, G., Vriend, G., 2002. Increasing the precision of comparative models with YASARA NOVA–a self-parameterizing force field. Proteins 47, 393–402. https://doi.org/10.1002/prot.10104.
Lentz, J., Pan, F., Ng, S.S., Deininger, P., Keats, B., 2007. Ush1c216A knock-in mouse survives Katrina. Mutat. Res. 616, 139–144. https://doi.org/10.1016/j.mrfmmm.2006.11.006.
Liepinsh, E., Trexler, M., Kaikkonen, A., Weigelt, J., Bányai, L., Patthy, L., Otting, G., 2001. NMR structure of the LCCL domain and implications for DFNA9 deafness disorder. EMBO J. 20, 5347–5353. https://doi.org/10.1093/emboj/20.19.5347.
Mianné, J., Chessum, L., Kumar, S., Aguilar, C., Codner, G., Hutchison, M., Parker, A., Mallon, A.M., Wells, S., Simon, M.M., Teboul, L., Brown, S.D.M., Bowl, M.R., 2016. Correction of the auditory phenotype in C57BL/6N mice via CRISPR/Cas9-mediated homology directed repair. Genom. Med. 8, 16. https://doi.org/10.1186/s13073-016-0273-4.
Newton, S., Kong, F., Carlton, A.J., Aguilar, C., Parker, A., Codner, G.F., Teboul, L., Wells, S., Brown, S.D.M., Marcotti, W., Bowl, M.R., 2022. Neuroplastin genetically interacts with Cadherin 23 and the encoded isoform Np55 is sufficient for cochlear hair cell function and hearing. PLoS Genet. 18, e1009937 https://doi.org/10.1371/journal.pgen.1009937.
Ohlemiller, K.K., 2019. Mouse methods and models for studies in hearing. J. Acoust. Soc. Am. 146, 3668–3680. https://doi.org/10.1121/1.5132550.
Ohlemiller, K.K., Jones, S.M., Johnson, K.R., 2016. Application of mouse models to research in hearing and balance. J. Assoc. Res. Otolaryngol. 17, 493–523. https://doi.org/10.1007/s10162-016-0589-1.
Pfaffl, M.W., Tichopad, A., Prgomet, C., Neuvians, T.P., 2004. Determination of stable housekeeping genes, differentially regulated target genes and sample integrity: bestKeeper – excel-based tool using pair-wise correlations. Biotechnol. Lett. 26, 509–515. https://doi.org/10.1023/b:bile.0000019559.84305.47.
Reese, M.G., Eeckman, F.H., Kulp, D., Haussler, D., 1997. Improved splice site detection in genie. J. Comput. Biol. 4, 311–323. https://doi.org/10.1089/cmb.1997.4.311.
Reiss, L.A.J., Kirk, J., Claussen, A.D., Fallon, J.B., 2022. Animal models of hearing loss after cochlear implantation and electrical stimulation. Hear. Res. 426, 108624 https://doi.org/10.1016/j.heares.2022.108624.
Rivolta, M.N., Grix, N., Lawlor, P., Ashmore, J.F., Jagger, D.J., Holley, M.C., 1998. Auditory hair cell precursors immortalized from the mammalian inner ear. Proc. Biol. Sci. 265, 1595–1603. https://doi.org/10.1098/rspb.1998.0477.
Robertson, N.G., Hamaker, S.A., Patriub, V., Aster, J.C., Morton, C.C., 2003. Subcellular localisation, secretion, and post-translational processing of normal cochlin, and of mutants causing the sensorineural deafness and vestibular disorder, DFNA9. J. Med. Genet. 40, 479–486. https://doi.org/10.1136/jmg.40.7.479.
Robertson, N.G., Jones, S.M., Sivakumaran, T.A., Giersch, A.B.S., Jurado, S.A., Call, L.M., Miller, C.E., Maison, S.F., Liberman, M.C., Morton, C.C., 2008. A targeted Coch missense mutation: a knock-in mouse model for DFNA9 late-onset hearing loss and vestibular dysfunction. Hum. Mol. Genet. 17, 3426–3434. https://doi.org/10.1093/hmg/ddn236.
Roosing, S., Lamers, I.J., Vrieze, E.de, Born, L.I.van den, Lambertus, S., Arts, H.H., Peters, T.A., Hoyng, C.B., Kremer, H., Hetterschijt, L., Letteboer, S.J., Wijk, E.van, Roepman, R., Hollander, A.I.den, Cremers, F.P., 2014. Disruption of the basal body protein POC1B results in autosomal-recessive cone-rod dystrophy. Am. J. Med. Genet. 95, 131–142. https://doi.org/10.1016/j.ajhg.2014.06.012. American Journal of Medical Genetics.
Schellens, R., Vrieze, E.de, Slijkerman, R., Kremer, H., Wijk, E.van, 2022. Antisense RNA design, delivery, and analysis. Methods Mol. Biol. 2434, 281–299. https://doi.org/10.1007/978-1-0716-2010-6_19.
Schrauwen, I., Hasin-Brumshtein, Y., Corneveaux, J.J., Ohmen, J., White, C., Allen, A.N., Lusis, A.J., Camp, G.V., Huentelman, M.J., Friedman, R.A., 2016. A comprehensive catalogue of the coding and non-coding transcripts of the human inner ear. Hear. Res. 333, 266–274. https://doi.org/10.1016/j.heares.2015.08.013.
Shan, A., Ting, J.S., Price, C., Goman, A.M., Willink, A., Reed, N.S., Nieman, C.L., 2020. Hearing loss and employment: a systematic review of the association between hearing loss and employment among adults. J. Laryngol. Otol. 134, 387–397. https://doi.org/10.1017/s0022215120001012.
Slijkerman, R., Goloborodko, A., Broekman, S., Vrieze, E.de, Hetterschijt, L., Peters, T.A., Gerits, M., Kremer, H., Wijk, E.van, 2018. Poor splice-site recognition in a humanized zebrafish knockin model for the recurrent deep-intronic c.7595-2144A>G mutation in USH2A. Zebrafish zeb 2018, 1613. https://doi.org/10.1089/zeb.2018.1613.
Southwell, A.L., Warby, S.C., Carroll, J.B., Doty, C.N., Skotte, N.H., Zhang, W., Villanueva, E.B., Kovalik, V., Xie, Y., Pouladi, M.A., Collins, J.A., Yang, X.W., Franciosi, S., Hayden, M.R., 2013. A fully humanized transgenic mouse model of Huntington disease. Hum. Mol. Genet. 22, 18–34. https://doi.org/10.1093/hmg/dds397.
Tommaso, P.D., Moretti, S., Xenarios, I., Orobitg, M., Montanyola, A., Chang, J.M., Taly, J.F., Notredame, C., 2011. T-Coffee: a web server for the multiple sequence alignment of protein and RNA sequences using structural information and homology extension. Nucl. Acids Res. 39, W13–W17. https://doi.org/10.1093/nar/gkr245.
Tu, N.C., Friedman, R.A., 2018. Age-related hearing loss: unraveling the pieces. Laryngosc. Investig. Otolaryngol. 3, 68–72. https://doi.org/10.1002/lio2.134.
Van Rompaey, V., 2020. Making the case for research on disease-modifying treatments to tackle post-lingual progressive sensorineural hearing loss. Front Neurol 11, 290. https://doi.org/10.3389/fneur.2020.00290.
Varadi, M., Anyango, S., Deshpande, M., Nair, S., Natassia, C., Yordanova, G., Yuan, D., Stroe, O., Wood, G., Laydon, A., Žídek, A., Green, T., Tunyasuvunakool, K., Petersen, S., Jumper, J., Clancy, E., Green, R., Vora, A., Lutfi, M., Figurnov, M., Cowie, A., Hobbs, N., Kohli, P., Kleywegt, G., Birney, E., Hassabis, D., Velankar, S., 2021. AlphaFold Protein Structure Database: massively expanding the structural coverage of protein-sequence space with high-accuracy models. Nucleic Acids Res 50, D439–D444. https://doi.org/10.1093/nar/gkab1061.
Verdoodt, D., Camp, G.V., Ponsaerts, P., Rompaey, V.V., 2020. On the pathophysiology of DFNA9: effect of pathogenic variants in the COCH gene on inner ear functioning in human and transgenic mice. Hearing Res 401, 108162. https://doi.org/10.1016/j.heares.2020.108162.
Verdoodt, D., Peeleman, N., Szewczyk, K., Camp, G.V., Ponsaerts, P., Rompaey, V.V., 2021. Cochlin deficiency protects aged mice from noise-induced hearing loss. Int. J. Mol. Sci. 22, 11549. https://doi.org/10.3390/ijms222111549.
Wang, J., Shen, J., Guo, L., Cheng, C., Chai, R., Shu, Y., Li, H., 2019. A humanized mouse model, demonstrating progressive hearing loss caused by MYO6 p.C442Y, is inherited in a semi-dominant pattern. Hear. Res. 379, 79–88. https://doi.org/10.1016/j.heares.2019.04.014.
Watson, C.J., Tempel, B.L., 2013. A new Atp2b2 deafwaddler allele, dfw i5, interacts strongly with Cdh23 and other auditory modifiers. Hear. Res. 304, 41–48. https://doi.org/10.1016/j.heares.2013.06.003.
WHO, 2023. Deafness and hearing loss WHO fact sheet [WWW Document]. Deafness and hearing loss WHO fact sheet. URL https://www.who.int/news-room/fact-sheets/detail/deafness-and-hearing-loss.
Xiong, W., Wagner, T., Yan, L., Grillet, N., Müller, U., 2014. Using injectoporation to deliver genes to mechanosensory hair cells. Nat. Protoc. 9, 2438–2449. https://doi.org/10.1038/nprot.2014.168.
Yao, J., Py, B.F., Zhu, H., Bao, J., Yuan, J., 2010. Role of protein misfolding in DFNA9 hearing loss. J.Biol. Chem. 285, 14909–14919. https://doi.org/10.1074/jbc.m110.106724.
Yariz, K.O., Duman, D., Seco, C.Z., Dallman, J., Huang, M., Peters, T.A., Sirmaci, A., Lu, N., Schraders, M., Skromne, I., Oostrik, J., Diaz-Horta, O., Young, J.I., Tokgoz-Yilmaz, S., Konukseven, O., Shahin, H., Hetterschijt, L., Kanaan, M., Oonk, A.M.M., Edwards, Y.J.K., Li, H., Atalay, S., Blanton, S., DeSmidt, A.A., Liu, X.Z., Pennings, R.J.E., Lu, Z., Chen, Z.Y., Kremer, H., Tekin, M., 2012. Mutations in OTOGL, encoding the inner ear protein otogelin-like, cause moderate sensorineural hearing loss. Am. J. Hum. Genet. 91, 872–882. https://doi.org/10.1016/j.ajhg.2012.09.011.